Ice Cloud Properties From Himawari-8/AHI Next-Generation Geostationary Satellite: Capability of the AHI to Monitor the DC Cloud Generation Process

Husi Letu, Takashi M. Nagao, Takashi Y. Nakajima, Jérôme Riedi, Hiroshi Ishimoto, Anthony J. Baran, Huazhe Shang, Miho Sekiguchi, and Maki Kikuchi

***Abstract*— The Japan Meteorological Agency (JMA) successfully launched the Himawari-8 (H-8) new-generation geostationary meteorological satellite with the Advanced Himawari Imager (AHI) sensor on October 7, 2014. The H-8/AHI level-2 (L2) operational cloud property products were released by the Japan Aerospace Exploration Agency during September 2016. The Voronoi light scattering model, which is a fractal ice particle habit, was utilized to develop the retrieval algorithm called "Comprehensive Analysis Program for Cloud Optical Measurement" (CAPCOM-INV)-ice for the AHI ice cloud product. In this paper, we describe the CAPCOM-INV-ice algorithm for ice cloud products from AHI data. To investigate its retrieval performance, retrieval results were compared with 2000 samples of the ice cloud optical thickness and effective particle radius values. Furthermore, AHI ice cloud products are evaluated by comparing them with the MODIS collection-6 (C6) products. As an experiment, cloud property retrievals from AHI measurements, with an observation interval time of 2.5 min and ground-based rainfall observation radar data (the latter of which is supplied by the JMA, with a 1-km grid mesh), are used to investigate the generation processes of deep convective (DC) cloud in the vicinity of the Kyushu island, Japan. It revealed that AHI measurements have the capability of monitoring the growth processes, including variation of the cloud properties and the precipitation in the DC cloud.**

***Index Terms*— DC cloud, ice clouds, remote sensing, retrieval algorithm.**

Manuscript received July 28, 2018; revised October 22, 2018; accepted November 11, 2018. Date of publication December 17, 2018; date of current version May 28, 2019. This work was supported in part by the National Key Research and Development Program of China under Grant 2018YFA0605401, in part by the National Natural Science Foundation of China under Grant 41771395, and in part by JST CREST, Japan, under Grant JPMJCR15K4. *(Corresponding author: Husi Letu.)*

H. Letu is with the State Key Laboratory of the Science and Remote Sensing, Institute of Remote Sensing and Digital Earth, Chinese Academy of Sciences, Beijing 100101, China, and also with the Research and Information Center, Tokai University, Tokyo 151-0063, Japan (e-mail: husiletuw@hotmail.com).

T. M. Nagao is with the Earth Observation Research Center, Japan Aerospace Exploration Agency, Tsukuba 305-8505, Japan.

T. Y. Nakajima is with the Research and Information Center, Tokai University, Tokyo 151-0063, Japan.

J. Riedi is with the Laboratoire d'Optique Atmosphérique, Université de Lille-Sciences et Technologies, 59655 Villeneuve d'Ascq, France.

H. Ishimoto is with the Meteorological Research Institute, Japan Meteorological Agency, Tsukuba 305-0052, Japan.

A. J. Baran is with the Met Office, Exeter EX1 3PB, U.K., and also with the School of Physics, Astronomy and Mathematics, University of Hertfordshire, Hatfield AL10 9AB, U.K.

H. Shang is with the State Key Laboratory of the Science and Remote Sensing, Institute of Remote Sensing and Digital Earth, Chinese Academy of Sciences, Beijing 100101, China.

M. Sekiguchi is with the Atmospheric and Environmental Physics Laboratory, Tokyo University of Marine Science and Technology, Tokyo 135-8533, Japan.

M. Kikuchi is with the Earth Observation Research Center, Japan Aerospace Exploration Agency, Tsukuba 305-8505, Japan.

Color versions of one or more of the figures in this paper are available online at http://ieeexplore.ieee.org.

Digital Object Identifier 10.1109/TGRS.2018.2882803

I. Introduction

HIMAWARI-8 (H-8) is a next-generation geostationary meteorological satellite that was successfully launched by the Japan Meteorological Agency (JMA) on October 7, 2014. H-8 operates at approximately 140° East, covering the East Asian and Western Pacific regions. The Advanced Himawari Imager (AHI) onboard the satellite has been significantly enhanced from the conventional geostationary satellite sensor (MTSAT-2), and the European Meteosat Second Generation series, in terms of its spectral coverage and temporal resolution [1]. The AHI possesses comparable capabilities to the GOES-R [2], [3] in terms of its spatial, spectral, and temporal resolutions (Table 1). The AHI provides near-global coverage of high-temporal and high-spatial cloud observations. The instrument has 16 observational bands, spanning from the visible to thermal infrared spectral regions with a nadir spatial resolution of 0.5 km (one band), 1 km (two bands), and 2 km (13 bands). The observation intervals are 10 and 2.5 min for the full disk (FLDK) region and the surrounding area (RRS) of Japan [4]. The AHI measurements in the visible, shortwave infrared, and thermal infrared bands (e.g., center wavelength at 0.68, 2.2, and 11 μm) are useful for retrieving cloud properties, such as the cloud optical thickness (COT), the effective particle radius (CER) and the cloud-top temperature (CTT).

Ice cloud property products from satellite measurements are widely applied to monitor climate change, numerical weather prediction, and meteorological disasters. However, there are still large uncertainties, especially in the cloud properties, that are mainly caused by the ice particle scattering (IPS) assumptions applied in the retrievals [5]–[7]. In comparison with liquid water cloud, optical and microphysical properties of ice clouds tend to be affected by the assumed IPS model, owing to the complex nature of nonspherical ice particles. The complex features of ice clouds contribute to the large

TABLE I
BAND SPECIFICATIONS OF THE H-8/AHI

Center wavelength(μm)	Himawari-8(AHI) (Spatial resolution/km)		MTSAT-1R/2 (Spatial resolution/km		MTG (Spatial resolution/km		GOES-R (ABI) (Spatial resolution/km)	
0.46	●	1			●	1	●	1
0.51	●	1			●			
0.64	●	0.5	●	1	●	1:05*	●	0.5
0.86	●	1			●	1	●	1
0.96					●			
1.3					●		●	2
1.6	●				●		●	1
2.3	●				●	1:0.5*	●	
3.9	●		●		●	2:1	●	
6.2	●		●	4	●	2	●	
7	●						●	
7.3	●	2			●	2	●	2
8.6	●				●		●	
9.6	●				●		●	
10.4	●		●	4	●	2:1*	●	
11.2	●						●	
12.3	●		●	4	●	2	●	
13.3	●				●		●	
Operation	FLDK(10min.): RRS(2.5 min.)					FLDK(10min.): RRS*(2.5min.)	1)Continuous FLDK:FLDK(5min.) 2)Flex mode FLDK(15min.): Meso(0.5min.): CONUS(5min.)	

(FLDF : Full Disk; Meso: Mesoscale; RRS : Regional-Rapid-Scan: CONUS: Continental US Flex: Flex Mode; * : The resolution of RRS observation)

uncertainties in the cloud radiative impacts, including ice particle surface roughness [8]. However, previous studies have [9]–[17] proposed a method of selecting the optimal IPS model using multiangle cloud observation measurements that enable more accurate retrievals of ice cloud microphysical properties. Generally, previous studies have found that IPS models with rough surfaces, including air bubbles or seriously aggregated habits, are the most appropriate models for retrievals of the optical and microphysical properties of ice clouds [18]. The works by [19] and [20] developed the single-scattering properties of the highly irregular ice particle model called the Voronoi aggregate (hereinafter referred to as the "Voronoi model") for generating ice cloud products of the Global Change Observation Mission—Climate (GCOM-C). Letu *et al.* [20] demonstrated that use of the Voronoi particle leads to a consistent set of ice cloud property retrievals in comparison with other well-known scattering models. These other models were the inhomogeneous monocrystal [15], [21], [22], the general habit mixture [23], [24], the five-plate aggregate [25], and ensemble ice particle models [12], [26]. Based on the results described in Letu *et al.* [20], we developed the AHI ice cloud property retrieval algorithm assuming the Voronoi model as representative of ice cloud scattering properties.

The AHI ice cloud retrieval algorithm is introduced in Section II. The accuracy of the ice cloud property products from the AHI is also investigated by comparing these results to the MODIS collection-6 (C6) cloud property products. Furthermore, the AHI cloud property data and radar measurements are collected to investigate the generation processes of the DC clouds with a 2.5-min observation time interval in Section III.

II. RETRIEVAL ALGORITHMS

Fig. 1 shows the spectral response function (SRF) for VIS and near-infrared response (NIR) bands for Himawari-8/AHI

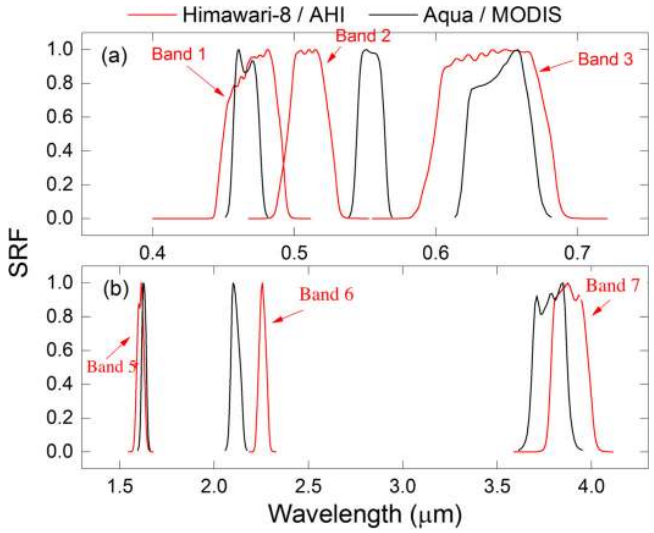

Fig. 1. SRFs for (a) VIS and (b) NIR for Himawari-8/AHI (red solid line) and Aqua/MODIS (black solid line).

and Aqua/MODIS. From Fig. 1, we can confirm that center wavelengths of the band 3 and band 5 in the AHI are similar to the center wavelength in the corresponding MODIS bands. There are three spectral bands at the shortwave infrared wavelength with center wavelength of 1.6, 2.3, and 3.9 μm, respectively. AHI measurements in band 3 and band 6 are selected to retrieve the cloud optical and effective particle radius for the AHI version β cloud property product. AHI level-2 cloud products, including ice cloud properties, are archived on the H-8 product homepage as "P-Tree" by the Japan Aerospace Exploration Agency (JAXA), from September 2015 to the present (http://www.eorc.jaxa.jp/ptree/index.html). The cloud screening algorithm developed by Ishida and Nakajima [27] and Nakajima *et al.* [28] has been employed to develop the AHI cloud mask and the thermodynamic phase product. The retrieval algorithm called the "Comprehensive Analysis Program for Cloud Optical Measurement" (CAPCOM-INV), developed by Nakajima and Nakajma [29] and Kawamoto *et al.* [30], is employed to develop the AHI warm water cloud product. The single-scattering properties of the water clouds are calculated using Lorenz–Mie theory in the CAPCOM-INV algorithm. The log-normal particle size distribution (PSD) is assumed to express the particle size spectrum of the water cloud in the algorithm. The CAPCOM-INV algorithm was improved (CAPCOM-INV-ice) to retrieve the optical and microphysical properties of the ice clouds by employing the Voronoi IPS model instead of the Lorenz–Mie scattering kernel as the kernel of the retrieval package for developing the AHI ice cloud product. The CAPCOM-INV-ice algorithm is selected as a standard algorithm for developing the ice cloud property products of the H-8/AHI, GCOM-C/SGLI, and the Earth Clouds, Aerosol and Radiation Explorer/Multispectral imager satellite program [20], [31].

The single-scattering properties of the IPS model are an important component of the forward RTM in simulation of ice cloud radiative properties. Fig. 2 indicates the comparison of the phase function between Voronoi model and eight-solid column aggregates with severely rough model used in

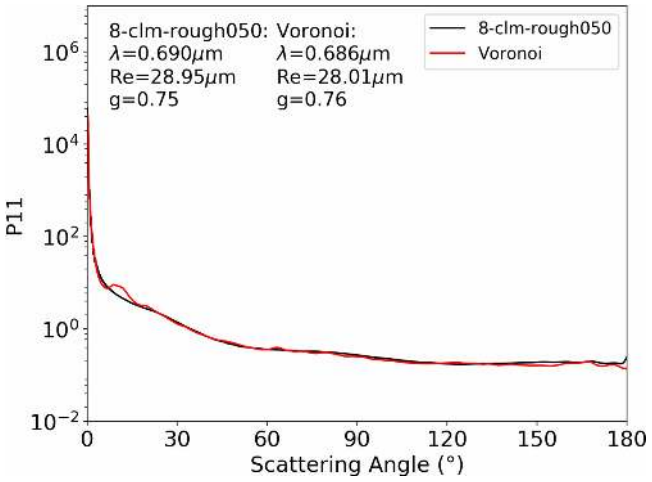

Fig. 2. Comparison of the phase function between Voronoi model and eight-solid column aggregates with severely rough model used in MODISD-C6 (λ: wavelength, Re: half length of the particle Max dimension, g: asymmetry factor).

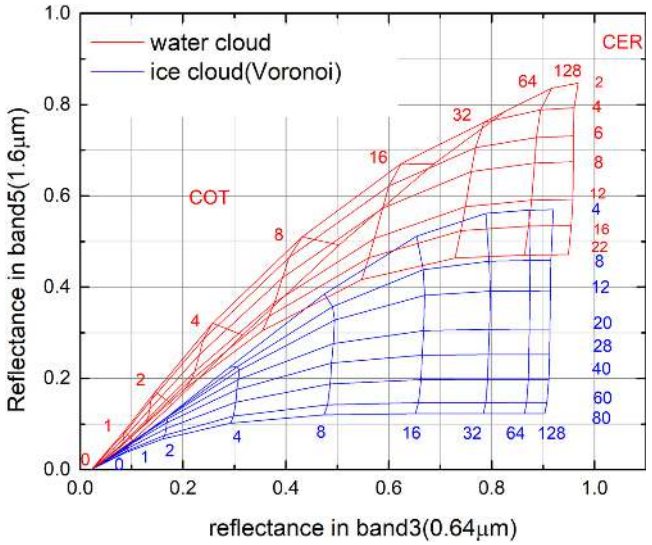

Fig. 3. Reflectance LUTs for water and ice clouds (Voronoi model) on AHI nonabsorbing channel (band 3) and absorbing channel (band 5). (U.S. standard atmospheric model, ground albedo = 0.1°, θsun = 30°, θsat = 30°, φ = 120).

MODISD-C6 at 0.69 μm. From Fig. 2, we can see that both the phase function (P11) and asymmetry factor (g) for the two models are similar in general. The asymmetry factors at the selected wavelength are 0.75 and 0.76, respectively. Fig. 3 shows reflectance of the water (red line) and ice clouds (blue line) with various COTs and CERs at top of the atmosphere by the AHI nonabsorbing (band 3) and weakly absorbing channels (band 5). Since shapes of the SRF in band 3 and band 5 of the AHI are similar to the corresponding MODIS bands (see Fig. 1), we selected the AHI data in center wavelength of 0.64 and 1.6 μm to retrieve the ice cloud for comparing MODIS-C6 product. From Fig. 3, we can confirm that the sensitivity of the reflectance in band 5 to particle size decreases significantly as CER values increase past 60 μm. It is also indicated that water cloud reflectance in band 5 is obviously different to ice cloud reflectance simulated by the

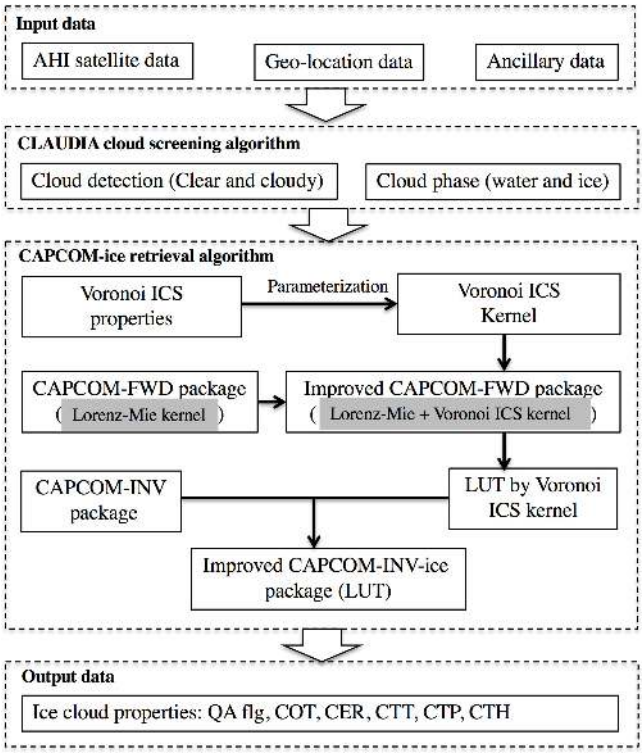

Fig. 4. Flowchart of the CAPCOM-INV-ice retrieval algorithm.

Voronoi model. However, selecting the optimal ice particle model to be used in the forward RTM model is important to improve the retrieval accuracy of the ice cloud properties. The Voronoi ice particle habit is determined by analyzing the many observations of ice crystal microphysical properties from aircraft *in situ* observations [19]. The Voronoi IPS model is developed using the following light scattering calculation methods: the finite difference time-domain (FDTD), geometric optics integral equation (GOIE), and the ray-tracing geometric optics method (GOM). The IPS properties include the geometrical cross section, phase function, extinction efficiency, absorption efficiency, single-scattering albedo, and the asymmetry factor. The FDTD code developed by Ishimoto *et al.* [19] is applied to calculate the database with size parameters ranging from approximately 0.3 to 30. The GOIE and GOM codes developed by Ishimoto *et al.* [19] and Masuda *et al.* [32] are used to compute the scattering database for ice particles with size parameters ranging from approximately 30 to 500 and those larger than 500, respectively. A detailed description of the accuracy of the Voronoi IPS database is described in [20]. The CER and PSDs of the ice particles are important parameters for the retrieval of ice cloud properties. The parameters used here were previously defined by Letu *et al.* [20] and are utilized in this paper, to improve the CAPCOM-INV-ice algorithm for developing the AHI ice cloud product. As shown in (1), ice cloud CER is defined as the radii of the equivalent volume spheres for the Voronoi habit particle. Single particle volume of the IPS model is provided by the Voronoi single-scattering property database

$$r_{\text{eff}} = \frac{3}{4}\frac{\int_0^\infty \text{Vol}(L)n(L)\text{DL}}{\int_0^\infty \text{Are}(L)n(L)\text{DL}} \tag{1}$$

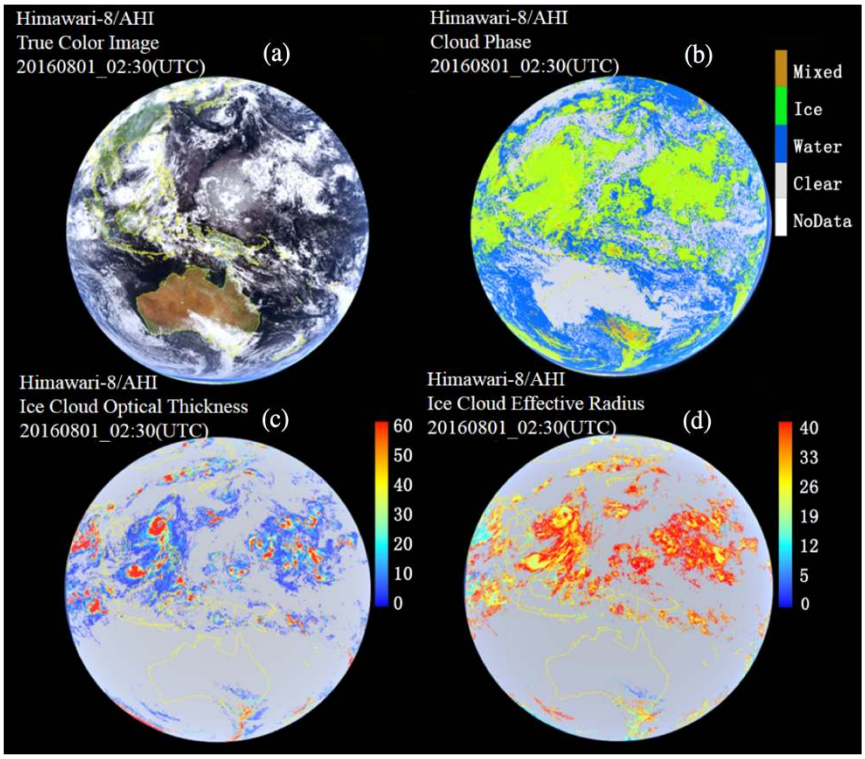

Fig. 5. (a) RGB composition image, (b) CPH, (c) ice cloud COT, (d) ice cloud CER from AHI data at 02:30 UTC, August 1, 2016.

where Vol(L) and Are (L) indicate the volume and equivalent sphere area of the Voronoi particle, respectively; L is the maximum dimension of the Voronoi particle; $n(L)$ is the PSD of the ice cloud particles as a function of the log-normal distribution function as shown in the following equation is used in the calculation fo the ice cloud CER:

$$n(\mathrm{re}) = \frac{N}{\sqrt{2\pi}\,\sigma} \exp\left[-\frac{(\ln \mathrm{re} - \ln r_0)^2}{2\sigma^2}\right] \tag{2}$$

where r_0 is the mode radius and σ is the log standard deviation of the size distribution.

The radiance reflected and emitted by the cloud layer in the visible and at the near-infrared wavelength (3) can be calculated by radiative transfer theory. Nakajima and Nakajima [29] employed the solar reflectance method to retrieve the optical thickness and effective particle radius of warm water clouds by establishing the precalculated lookup table (LUT) method using an assumed radiative transfer model (RTM) [33], [34]. In the retrieval method, the operation is repeated until the differences between the satellite measurements in all channels and LUT values are less than 0.1% using the Newton–Raphson method

$$R(\tau, r_e; \mu, \mu_0, \phi) = R_{\mathrm{obs}}(\tau, r_e; \mu, \mu_0, \phi) - t(\tau, r_e; \mu) \times \frac{A_g}{1 - \bar{r}(\tau, r_e) A_g} t(\tau, r_e; \mu_0) \frac{\mu_0 F_0}{\pi} \tag{3}$$

where F_0 is the extraterrestrial solar flux, τ, τ_c, and τ_u are, respectively, the optical thicknesses of atmosphere, cloud layer, and the atmosphere above the cloud layer, μ_0 and μ are, respectively, the cosines of solar and satellite zenith angles, and ϕ is the azimuthal angle of the satellite relative to the sun.

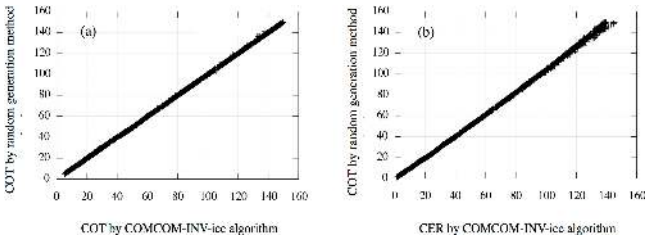

Fig. 6. Comparisons of the (a) COT and (b) CER from the random generation and CAPCOM-INV-ice retrieval algorithms (U.S. standard atmospheric model).

Fig. 4 shows the flowchart of the AHI ice cloud retrieval algorithm, H-8/AHI L1B data, geolocation data, and ancillary data, including the atmospheric reanalysis data, that were used in the CLAUDIA cloud screening algorithm to generate the cloud mask and cloud phase (CPH). The CLAUDIA cloud screening algorithm was developed by Ishida and Nakajima [27] and was adapted here to generate the cloud mask and CPH based on the channel specifications of the AHI sensor and the various solar viewing angles of the geostationary satellite. The input data and generated cloud mask and phase are input into the CAPCOM-INV-ice retrieval algorithm to generate the ice cloud COT, CER, CTT, CPH, and cloud-top height (CTH). Details of the CAPCOM-INV-ice algorithm are shown below. The single-scattering IPS database of the Voronoi habit model was developed based on the channel specifications of the AHI sensor. Then, the scattering property database was utilized to develop the Voronoi IPS kernel for its use in the forward RTM, called CAPCOM-FWD [29]. The Voronoi kernel was installed in CAPCOM-FWD to calculate the LUTs for the CAPCOM-INV-ice algorithm. The LUTs for the AHI ice

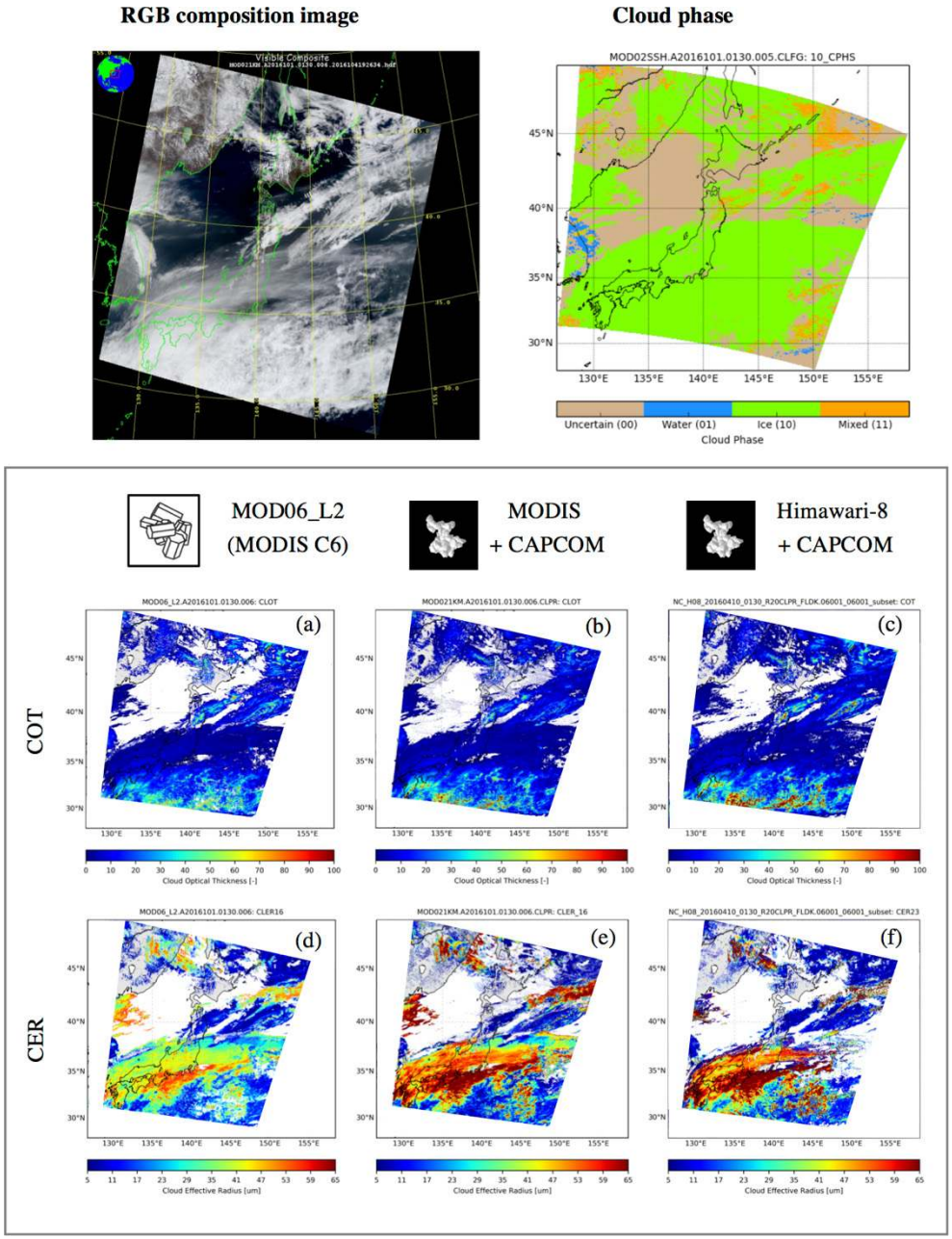

Fig. 7. (Top) True-color composite image and CPH. (Bottom) Comparison of the ice cloud optical and microphysical properties derived from the MODIS and AHI data from the same observation time of 01:30 UTC, April 10, 2016. (a) COT derived from the MODIS C6 product. (b) COT derived from the MODIS L1B data. (c) COT derived from the H-8 data. (d) CER derived from the MODIS C6 product. (e) CER derived from the MODIS L1B data. (f) CER derived from the H-8 data.

cloud retrieval algorithm were calculated via the established CAPCOM-FWD using the response functions of the AHI channels. The LUT was implemented in the CAPCOM algorithm to complete the CAPCOM-INV-ice algorithm. Finally, the ice cloud properties, including the quality assurance flag for multilayer cloud, are retrieved from H-8/AHI L1B data using the CAPCOM-INV-ice algorithm.

III. Results and Discussion

A. Performance Check of the Algorithm and AHI Ice Cloud Properties

Fig. 5 shows the true-color composite image, CPH and ice cloud COT and CER from the AHI measurement at 02:30 UTC, August 1, 2016. The AHI is the first geostationary satellite sensor capable of generating a true-color composite image. Fig. 5(a) allows us to confirm the cloud distributions for the FLDK of the observation region, which includes East and South Asia, Oceania, the Western Pacific Ocean, and part of the Indian Ocean. Most of the region is covered by water and ice clouds [Fig. 5(b)]. Water clouds are mainly distributed over the Arctic and southern hemisphere, whereas ice clouds are mostly distributed over the Pacific Ocean in the northern hemisphere and partly over the Antarctic. Mixed-phase clouds are sparsely distributed in the south of Oceania over the Indian Ocean. In this paper, the optical and microphysical properties of the mixed-phase clouds are retrieved

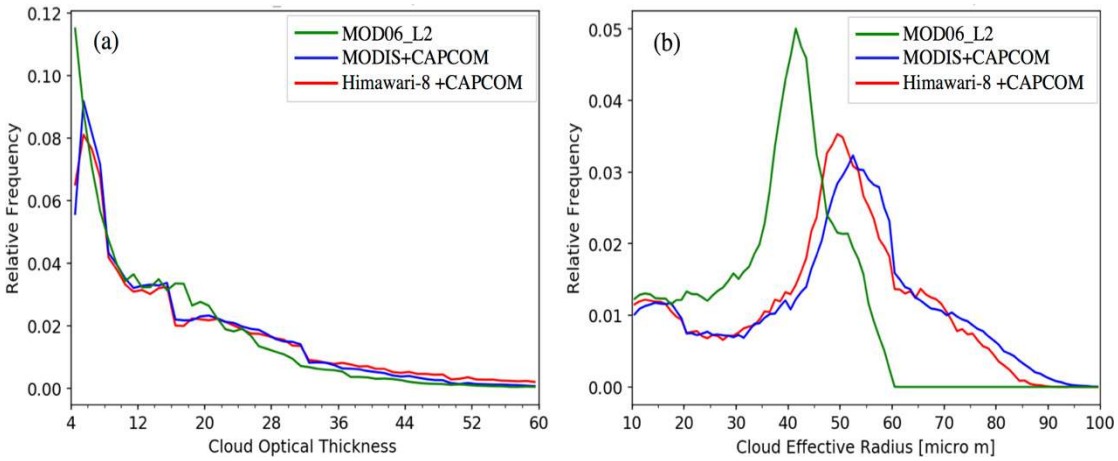

Fig. 8. PDF of the COT and CER in Fig. 7.

by the CAPCOM-INV-ice algorithm using the Voronoi model. Fig. 5(c) and (d) shows the distributions of the COT and CER of the ice clouds, respectively. From the Fig. 5, we can confirm that there is a typhoon over the South China Sea.

To test the performance of the CAPCOM-INV-ice retrieval algorithm, we simulated the COT and CER of the ice clouds for 2000 samples using the observation geometry (e.g., the zenith angle of the satellite and sun and the relative azimuth angle). The generated parameters were then input into the CAPCOM-FWD forward model to calculate the satellite-observed radiance. A random generation function in the Fortran program was used to simulate the COT and CER of the ice cloud. We then input the calculated radiances in the CAPCOM-INV-ice algorithm to retrieve the COT and CER. Finally, we compared the COT and CER from the retrieval results with the simulated results.

Fig. 6 shows the comparison of the COT and CER using the simulations and the CAPCOM-INV-ice retrieval algorithm. The maximum values of the COT and CER in the simulations are set to 160, based on the parameter setting within the AHI ice cloud product. Moreover, the Voronoi model is applied in the CAPCOM-FWD forward model to simulate the ice cloud properties. Fig. 6 shows that the COT [Fig. 6(a)] and CER [Fig. 6(b)] of the ice cloud from the simulations and retrieval algorithm fit well to the 1:1 line. Using the performance test, we can confirm that the CAPCOM-INV-ice algorithm is suitable for retrieving the ice cloud properties from the satellite measurements.

B. Comparison of the Ice Cloud Properties Derived From the AHI and MODIS Measurements

To investigate the accuracy of the AHI ice cloud product, the retrieval results obtained using the CAPCOM-INV-ice algorithm are compared to the MODIS-C6 cloud product. Fig. 7 (top) shows the true-color composite image and CPH of the surrounding area of Japan at 01:30 UTC, April 10, 2016. From the CPH, we can confirm that most of the selected area is covered by ice clouds. Fig. 7 (bottom) shows the IPS habit model (top row), the COT and CER from the MODIS-C6 cloud property product, the MODIS L1B data, and the AHI L1 data in band 3 and band 5 retrieved by the CAPCOM-INV-ice algorithm. Fig. 8 presents the probability density function (PDF) of the COT and CER from the MODIS and AHI measurements in Fig. 7, respectively. The shapes of the PDFs depend on the types of satellite data and the IPS model. Table II shows the "MODIS_L2 (MODIS C6)" in Fig. 7 and implies that the IPS model was used in the C6 product [Fig. 7(a) and (d)]; "MODIS + CAPCOM" implies that the Voronoi model was used in the CAPCOM-INV-ice algorithm to retrieve the MODIS ice cloud properties [Fig. 7(b) and (e)]; and last, "Himawari-8 + CAPCOM" implies that the Voronoi model was used in the CAPCOM-INV-ice algorithm to retrieve the AHI ice cloud properties [i.e., Fig. 7(c) and (f)].

Fig. 7 shows that the COT from MODIS-C6 [Fig. 7(a)] agrees well with the results from the MODIS L1B data [Fig. 7(b)]. From Fig. 8(a), we can also confirm that the COTs from these two products are similar in general. However, the COT from AHI data [Fig. 7(c)] in the southern part of the image with higher values (dark red region) and COT from MODIS L1B by CAPCOM-INV-ice algorithm [Fig. 7(b)] show some differences, even though these COTs are retrieved using the same algorithm. The reason for these differences is related to the AHI instrument being in geostationary orbit. Thus, the viewing angle of this sensor is significantly different from those of the polar orbiting satellites (e.g., MODIS) in higher latitude regions. Since natural clouds are inhomogeneous in the 3-D structures and also vertically [35]–[39], it is plausible to postulate that different viewing angles of the two sensors result in different COT retrievals.

As shown in Fig. 7(d) and (e), the CERs from both products differ significantly in the ice cloud region. From Fig. 8(b), we can also confirm that CER from MODIS-C6 (green line) is significantly smaller than results from MODIS L1B data (blue line). One source for the differences could be the definitions adopted for the CER and the PSD for the AHI cloud properties. The definition adopted for AHI is different from the gamma PSD employed for the MODIS retrievals. Another reason for these differences being considered is that the IPS model employed to produce the MODIS-C6 ice cloud properties is assumed to be an aggregated solid column with a rough surface (Ag-CLM-rough) [40], which is different from the Voronoi model employed in the MODIS L1B cloud property

TABLE II
ILLUSTRATION OF THE IPS MODEL IN FIG. 4

Data Source	MODIS_L2 (MODIS C6)	MODIS+ CAPCOM	Himawari-8+ CAPCOM
ICS model	Ag-CLM-rough*	Voronoi	Voronoi
Retrieval algorithm	MODIS C6	CAPCOM-INV-ice	CAPCOM-INV-ice
Satellite data	MODIS	MODIS	AHI

(*Ag-CLM-rough: aggregated solid column with a rough surface)

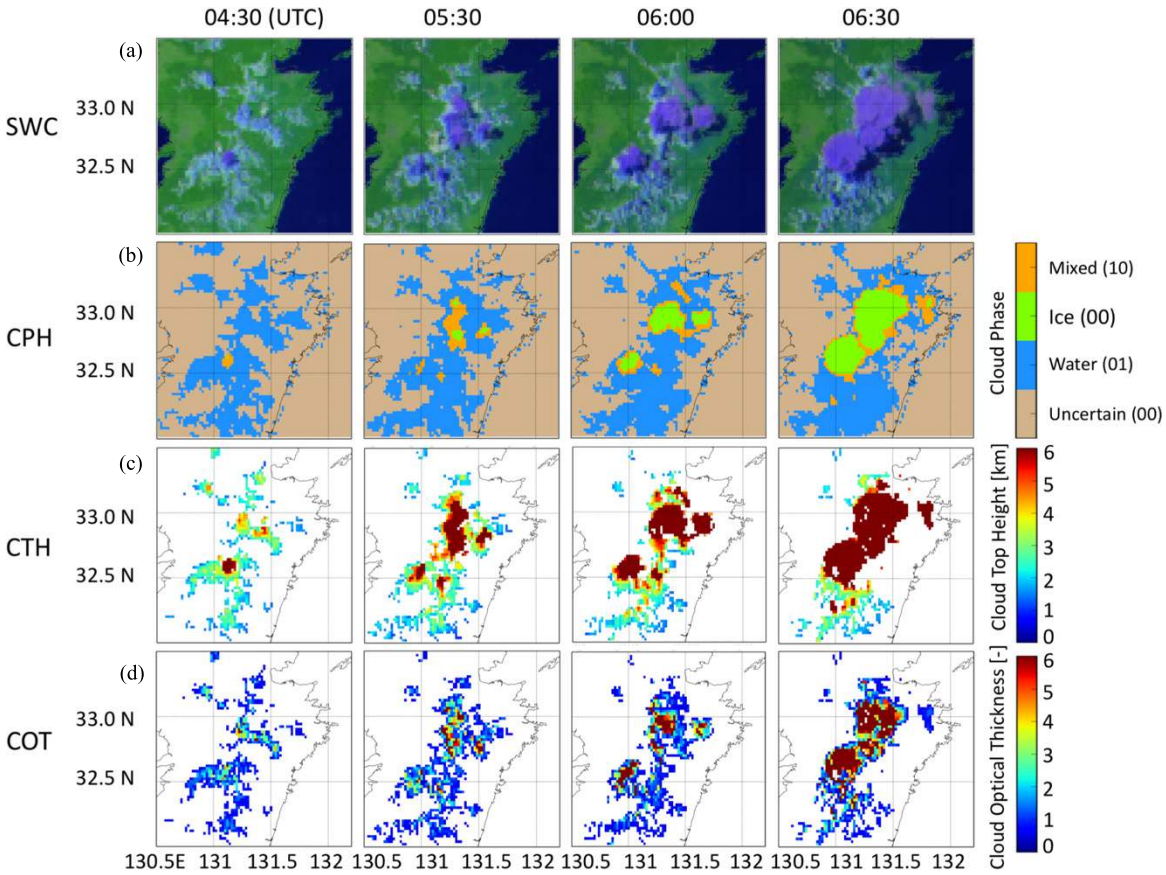

Fig. 9. Time-series false-color composition image (R: 2.1 μm, G: 1.6 μm, B: 0.64 μm) and microphysical cloud properties from the AHI measurements with 2. thickness, and 5-min observation frequencies over Kyusyu Island, Japan on August 1, 2016. (a) False-color composition imagery of Kyusyu Island, (b) CPH, (c) optical, and (d) cloud-top pressure.

retrievals by CAPCOM-INV-ice algorithm. This difference in the IPS model results in geometries of the AHI and the MODIS instruments, for the same reasons as found for the differences of the retrieved COT in Fig. 7(b) and(c).

C. Experiments: Applications of the DC Cloud Generation Process Analysis

The comprehensive cloud properties estimated from satellite data are crucial for monitoring the dc clouds, which are complex and fast changing. The generation process of DC clouds is difficult to observe using the polar orbiting and traditional Geostationary Meteorological Satellites (GMS). Although conventional GMS measurements make it possible to capture the variations of the DC clouds, observing the detailed variations of the optical and microphysical properties remains difficult, as the instrument is limited by the temporal, spatial, and spectral (TSS) resolutions of its sensors. Ground-based rainfall observation radar has the ability to monitor DC cloud generation processes. However, positioning the instrument over ocean and mountainous areas remains a challenge. Since the TSS resolutions of the AHI measurements is very high, the measurements can be utilized to calculate the rapidly changing cloud parameters, such as the CPH, COT, and CTH, which are involved in the growth process of the dc cloud. Therefore, we choose to investigate whether the AHI measurem ents can replace the rainfall radar for observing

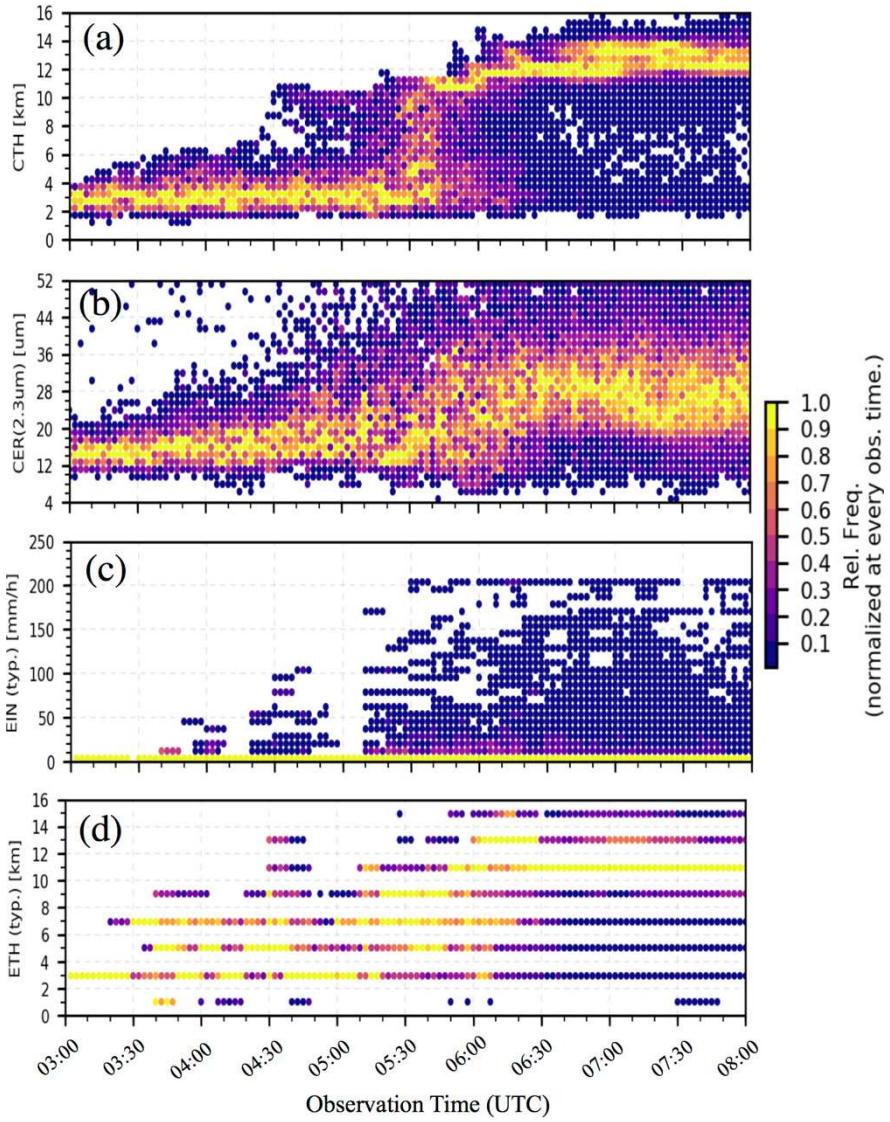

Fig. 10. JMA Doppler weather radar observation data from Kyusyu Island, Japan. (a) CTH from the AHI data. (b) Effective cloud radius from the AHI data,. (c) EIN from the JMA-Radar. (d) ETH from the JMA-Radar.

the cloud parameters in the DC cloud generation processes. To further investigate the DC cloud generation processes, the cloud properties from the AHI data are compared to the ground-based rainfall observation radar measurements by JMA (JMA-Radar).

Fig. 9 shows the false-color composite image (SWC), CPH, and cloud microphysical properties from the AHI measurements with a 2.5-min observation frequency obtained from above Kyushu Island, Japan. From the false-color composite image, shown in the top panel of the image, we can confirm that the expansion of the cloud area is obvious over time. The areal coverage of the CPH and COT increase with time, and the CTH increases significantly according to the growth of the DC cloud. The CPH change (from the water to ice phase) and obvious growth of the cloud area and COT, coincides with an increase in the CTH. Overall, the results in Fig. 9 suggest that AHI measurements can be used to monitor the detailed variations of the CPH, CTH, and optical properties of the dc cloud generation process.

Fig. 10(a) and (b) shows the CTH and CER as a function of observation time, which is derived from the AHI cloud product in the selected area, as shown in Fig. 9. Fig. 10(c) and (d) indicates the precipitation index of the echo intensity (EIN) and echo top height (ETH) from the JMA-Radar. The color bar in the image indicates the density of the image pixels in the observed data. EIN implies the intensity of precipitation, and ETH is defined as the maximum height of the minimum detectable echo [45], which implies the CTH in the target areas. Originally, the data of the ETH skip values in the altitude direction, such that there are blank values in the y-axis direction of Fig. 10(d). The JMA-Radar data with a 1-km mesh are obtained from the database server released by the Research Institute for Sustainable Humanosphere, Kyoto University (http://www.rish.kyoto-u.ac.jp/?lang=en).

Fig. 10(a) shows that the satellite-estimated CTH has increased sharply from 10 to 14 km with the growth of the DC clouds after the observation at 4:30. The CTH values of

most of the cloud pixels changed from 12 to 14 km between 5:30 and 08:00. In Fig. 10(b), the satellite-estimated CER for most of the cloud pixels ranged between 10 and 30 μm during 03:00–04:30. The CER increased significantly, reaching up to 50 μm after the observation at 05:30, due to the growth of the dc cloud. The CER values for most cloud pixels (implying the cloud area) ranged from 20 to 40 μm. In general, the CER of the ice cloud was larger than that for the water cloud. Accompanied by the dc cloud generation process, the CPHs changed from water to ice, which results in an obvious increase in the CER.

Fig. 10(c) shows that the intensity of the precipitation increases significantly, from 50 to 200 mm/h after the observation at 04:30. The cloud particles take time to grow into raindrops, so the peak value of the EIN appears more slowly than those of the CER and CTH. The ETH values increase from 3 to 13 km after the observation at 04:30, and the variation trend was similar to the CTH from the AHI measurements [Fig. 10(a)]. Overall, the cloud property parameters for the CER and CTH from the AHI data are consistent with the precipitation index of the EIN from the JMA-Radar observations. Since the radar observation data lack spatial information about the clouds and precipitation, the cloud property parameters from the AHI measurements are important for the interpretation of the variation characteristics of the cloud parameters and of the precipitation with the growth of the DC cloud.

IV. Conclusion

The AHI ice cloud optical and microphysical property products were introduced to provide a retrieval algorithm and asses the accuracy of the ice cloud products. The Voronoi scattering model is assumed in the CAPCOM-INV-ice retrieval algorithm to develop the AHI ice cloud products. To investigate the performance of the CAPCOM-INV algorithm, 2000 samples of the ice cloud COT and CER values were compared with retrieval results from the CAPCOM-INV algorithm. In these comparisons, selected COT and CER values were used to calculate the satellite-observed radiance for the further retrieval of the ice cloud parameters. As a result, both the simulated COT and CER and the retrieval algorithm fit well to the 1:1 line. The CAPCOM-INV-ice algorithm was demonstrated to be suitable to retrieve ice cloud properties from the AHI measurements.

The ice cloud properties of the COT and CER retrieved from the AHI measurements are compared to the MODIS-C6 ice cloud products to characterize the AHI ice cloud products. The results show that the COT from the AHI products agrees well with its counterpart from the MODIS C6 products. There are significant differences in the ice cloud CER values derived from MODIS C6 products and the MODIS L1B data, which are likely caused by the definition of the CER, PSD, and selected IPS model. The CER from the AHI products agrees well with the results from MODIS L1B data. The retrievals of the ice cloud COT are concluded to be less affected by both the satellite viewing angles and ice scattering models applied in the retrieval algorithms. The CER is easily affected by the definition of the CER, PSD, and IPS model, which is less affected by the satellite viewing angle.

Since the AHI sensor has a high temporal resolution, its values are easily matched with observations from other sensors. To investigate the capability of the AHI measurements for monitoring the precipitation processes with the growth of the DC cloud, the variations of the cloud properties derived from the AHI cloud products are compared with the precipitation data provided by the JMA-Radar on Kyushu Island, Japan. The variation characteristics of the CTT and CER from ground-based observations and AHI retrievals agree well.

This applied study indicates that the AHI ice cloud products can both provide the variations of the optical and microphysical properties of the ice clouds during the cloud generation process, and have the potential to allow the estimation of precipitation information, such as intensity and height. Our results are important for future studies of the DC cloud growth processes and applied studies using the AHI ice cloud products.

Acknowledgment

The Himawari-8 cloud property products used in this paper was supplied by the P-Tree System, Japan Aerospace Exploration Agency.

References

[1] K. Bessho *et al.*, "An introduction to Himawari-8/9—Japan's new-generation geostationary meteorological satellites," *J. Meteorol. Soc. Jpn.*, vol. 94, no. 2, pp. 151–183, 2016.

[2] T. J. Schmit, M. M. Gunshor, W. P. Menzel, J. J. Gurka, J. Li, and A. S. Bachmeier, "Introducing the next-generation advanced baseline imager on Goes-R," *Bull. Amer. Meteorol. Soc.*, vol. 86, no. 8, pp. 1079–1096, 2005.

[3] H. Iwabuchi *et al.*, "Cloud property retrieval from multiband infrared measurements by Himawari-8," *J. Meteorol. Soc. Jpn.*, vol. 96B, Jan. 2018, Art. no. 2018-001.

[4] Y. Kurihara, H. Murakami, and M. Kachi, "Sea surface temperature from the new Japanese geostationary meteorological Himawari-8 satellite," *Geophys. Res. Lett.*, vol. 43, no. 3, pp. 1234–1240, 2016.

[5] P. Yang *et al.*, " Spectrally consistent scattering, absorption, and polarization properties of atmospheric ice crystals at wavelengths from 0.2 to 100 μm," *J. Atmos. Sci.*, vol. 70, no. 1, pp. 330–347, Jan. 2013.

[6] P. Yang *et al.*, "On the radiative properties of ice clouds: Light scattering, remote sensing, and radiation parameterization," *Adv. Atmos. Sci.*, vol. 32, no. 1, pp. 32–63, 2015.

[7] Z. Zhang *et al.*, "Influence of ice particle model on satellite ice cloud retrieval: Lessons learned from MODIS and POLDER cloud product comparison," *Atmos. Chem. Phys.*, vol. 9, no. 18, pp. 7115–7129, 2009.

[8] B. Yi *et al.*, "Influence of ice particle surface roughening on the global cloud radiative effect," *J. Atmos. Sci.*, vol. 70, no. 9, pp. 2794–2807, 2013.

[9] A. J. Baran, P. D. Watts, and J. S. Foot, "Potential retrieval of dominating crystal habit and size using radiance data from a dual-view and multiwavelength instrument: A tropical cirrus anvil case," *J. Geophys. Res. Atmos.*, vol. 103, no. D6, pp. 6075–6082, 1998.

[10] A. J. Baran, P. D. Watts, and P. N. Francis, "Testing the coherence of cirrus microphysical and bulk properties retrieved from dual-viewing multispectral satellite radiance measurements," *J. Geophys. Res. Atmos.*, vol. 104, no. D24, pp. 31673–31683, 1999.

[11] A. J. Baran, S. Havemann, P. N. Francis, and P. D. Watts, "A consistent set of single-scattering properties for cirrus cloud: Tests using radiance measurements from a dual-viewing multi-wavelength satellite-based instrument," *J. Quant. Spectrosc. Radiat. Transf.*, vols. 79–80, no. 2, pp. 549–567, 2003.

[12] A. J. Baran and L. C. Labonnote, "A self-consistent scattering model for cirrus. I: The solar region," *Quart. J. Roy. Meteorol. Soc.*, vol. 133, no. 629, pp. 1899–1912, 2007.

[13] H. Chepfer, G. Brogniez, and Y. Fouquart, "Cirrus clouds' microphysical properties deduced from POLDER observations," *J. Quant. Spectrosc. Radiat. Transf.*, vol. 60, no. 3, pp. 375–390, 1998.

[14] A. J. Baran, S. Havemann, P. N. Francis, and P. D. Watts, "A consistent set of single-scattering properties for cirrus cloud: Tests using radiance measurements from a dual-viewing multi-wavelength satellite-based instrument," *J. Quant. Spectrosc. Radiat. Transf.*, vols. 79–80, no. 2, pp. 549–567, 2003.

[15] L.-C. Labonnote, G. Brogniez, M. Doutriaux-Boucher, J. C. Buriez, J. F. Gayet, and H. Gayet, "Modeling of light scattering in cirrus clouds with inhomogeneous hexagonal monocrystals. Comparison with *in-situ* and ADEOS-POLDER measurements," *Geophys. Res. Lett.*, vol. 27, no. 1, pp. 113–116, 2000.

[16] H. Chepfer, P. Goloub, J. Riedi, J. F. De Haan, J. W. Hovenier, and P. H. Flamant, "Ice crystal shapes in cirrus clouds derived from POLDER/ADEOS-1," *J. Geophys. Res. Atmos.*, vol. 106, no. D8, pp. 7955–7966, 2001.

[17] A. J. Baran and L. C. Labonnote, "On the reflection and polarisation properties of ice cloud," *J. Quant. Spectrosc. Radiat. Transf.*, vol. 100, nos. 1–3, pp. 41–54, 2006.

[18] C. Liu *et al.*, "A two-habit model for the microphysical and optical properties of ice clouds," *Atmos. Chem. Phys.*, vol. 14, no. 13, pp. 13719–13737, 2014.

[19] H. Ishimoto, K. Masuda, Y. Mano, N. Orikasa, and A. Uchiyama, "Irregularly shaped ice aggregates in optical modeling of convectively generated ice clouds," *J. Quant. Spectr. Rad. Trans.*, vol. 113, no. 8, pp. 632–643, 2012.

[20] H. Letu *et al.*, "Investigation of ice particle habits to be used for ice cloud remote sensing for the GCOM-C satellite mission," *Atmos. Chem. Phys.*, vol. 16, no. 18, pp. 12287–12303, 2016.

[21] L. C. Labonnote, G. Brogniez, J.-C. Buriez, M. Doutriaux-Boucher, J.-F. Gayet, and A. Macke, "Polarized light scattering by inhomogeneous hexagonal monocrystals: Validation with ADEOS-POLDER measurements," *J. Geophys. Res. Atmos.*, vol. 106, no. D11, pp. 12139–12153, 2001.

[22] M. Doutriaux-Boucher, J.-C. Buriez, G. Brogniez, L. C. Labonnote, and A. J. Baran, "Sensitivity of retrieved POLDER directional cloud optical thickness to various ice particle models," *Geophys. Res. Lett.*, vol. 27, no. 1, pp. 109–112, 2000.

[23] B. A. Baum *et al.*, "Ice cloud single-scattering property models with the full phase matrix at wavelengths from 0.2 to 100 μm," *J. Quant. Spectrosc. Radiat. Transf.*, vol. 146, pp. 123–139, Oct. 2014.

[24] B. A. Baum *et al.*, "Improvements in shortwave bulk scattering and absorption models for the remote sensing of ice clouds," *J. Appl. Meteorol. Climatol.*, vol. 50, no. 5, pp. 1037–1056, 2011.

[25] P. Yang *et al.*, "Spectrally consistent scattering, absorption, and polarization properties of atmospheric ice crystals at wavelengths from 0.2 to 100 μm," *J. Atmos. Sci.*, vol. 70, no. 1, pp. 330–347, 2013.

[26] A. J. Baran, P. Hill, K. Furtado, P. Field, and J. Manners, "A coupled cloud physics–radiation parameterization of the bulk optical properties of cirrus and its impact on the met office unified model global atmosphere 5.0 configuration," *J. Climate*, vol. 27, no. 20, pp. 7725–7752, 2014.

[27] H. Ishida and T. Y. Nakajima, "Development of an unbiased cloud detection algorithm for a spaceborne multispectral imager," *J. Geophys. Res. Atmos.*, vol. 114, no. D7, pp. 1291–1298, 2009.

[28] T. Y. Nakajima, T. Tsuchiya, H. Ishida, T. N. Matsui, and H. Shimoda, "Cloud detection performance of spaceborne visible-to-infrared multispectral imagers," *Appl. Opt.*, vol. 50, no. 17, pp. 2601–2616, 2011.

[29] T. Y. Nakajima and T. Nakajma, "Wide-area determination of cloud microphysical properties from NOAA AVHRR measurements for FIRE and ASTEX regions," *J. Atmos. Sci.*, vol. 52, no. 23, pp. 4043–4059, 1995.

[30] K. Kawamoto, T. Nakajima, and T. Y. Nakajima, "A global determination of cloud microphysics with AVHRR remote sensing," *J. Climate*, vol. 14, no. 9, pp. 2054–2068, 2001.

[31] H. Takenaka, T. Y. Nakajima, I. Okada, J. R. Dim, and T. Takamura, "Cloud optical thickness estimation from GMS-5/SVISSR," *J. Remote Sens. Soc. Jpn.*, vol. 29, no. 2, pp. 392–397, 2009.

[32] K. Masuda, H. Ishimoto, and Y. Mano, "Efficient method of computing a geometric optics integral for light scattering by nonspherical particles," *Papers Meteorol. Geophys.*, vol. 63, pp. 15–19, Feb. 2012.

[33] T. Nakajima and M. Tanaka, "Matrix formulations for the transfer of solar radiation in a plane-parallel scattering atmosphere," *J. Quant. Spectrosc. Radiat. Transf.*, vol. 35, no. 1, pp. 13–21, 1986.

[34] M. Sekiguchi and T. Nakajima, "A k-distribution-based radiation code and its computational optimization for an atmospheric general circulation model," *J. Quant. Spectrosc. Radiat. Transf.*, vol. 109, nos. 17–18, pp. 2779–2793, 2008.

[35] T. Y. Nakajima, K. Suzuki, and G. L. Stephens, "Droplet growth in warm water clouds observed by the A-train. Part II: A multisensor view," *J. Atmos. Sci.*, vol. 67, no. 6, pp. 1897–1907, 2010.

[36] T. Y. Nakajima, K. Suzuki, and G. L. Stephens, "Droplet growth in warm water clouds observed by the A-train. Part I: Sensitivity analysis of the MODIS-derived cloud droplet sizes," *J. Atmos. Sci.*, vol. 67, no. 67, pp. 1884–1896, 2010.

[37] Z. Zhang and S. Platnick, "An assessment of differences between cloud effective particle radius retrievals for marine water clouds from three MODIS spectral bands," *J. Geophys. Res. Atmos.*, vol. 116, no. D20, p. 215, 2011.

[38] Z. Zhang, A. S. Ackerman, G. Feingold, S. Platnick, R. Pincus, and H. Xue, "Effects of cloud horizontal inhomogeneity and drizzle on remote sensing of cloud droplet effective radius: Case studies based on large-eddy simulations," *J. Geophys. Res. Atmos.*, vol. 117, no. D19, p. 19208, 2012.

[39] T. M. Nagao, K. Suzuki, and T. Y. Nakajima, "Interpretation of multiwavelength-retrieved droplet effective radii for warm water clouds in terms of in-cloud vertical inhomogeneity by using a spectral bin microphysics cloud model," *J. Atmos. Sci.*, vol. 70, no. 8, pp. 2376–2392, 2013.

[40] S. Platnick *et al.*, "The MODIS cloud optical and microphysical products: Collection 6 updates and examples from Terra and Aqua," *IEEE Trans. Geosci. Remote Sens.*, vol. 55, no. 1, pp. 502–525, Jan. 2017.

[41] B. Yi, A. D. Rapp, P. Yang, B. A. Baum, and M. D. King, "A comparison of Aqua MODIS ice and liquid water cloud physical and optical properties between collection 6 and collection 5.1: Cloud radiative effects," *J. Geophys. Res. Atmos.*, vol. 122, no. 8, pp. 4550–4564, 2017.

[42] B. Yi, A. D. Rapp, P. Yang, B. A. Baum, and M. D. King, "A comparison of Aqua MODIS ice and liquid water cloud physical and optical properties between collection 6 and collection 5.1: Cloud radiative effects," *J. Geophys. Res. Atmos.*, vol. 122, no. 8, pp. 4550–4564, 2017.

[43] B. Yi, P. Yang, Q. Liu, P. Delst, S.-A. Boukabara, and F. Weng, "Improvements on the ice cloud modeling capabilities of the community radiative transfer model," *J. Geophys. Res.*, vol. 121, no. 22, 2016.

[44] B. Yi, A. D. Rapp, P. Yang, B. A. Baum, and M. D. King, "A comparison of Aqua MODIS ice and liquid water cloud physical and optical properties between collection 6 and collection 5.1: Pixel-to-pixel comparisons," *J. Geophys. Res. Atmos.*, vol. 122, no. 8, pp. 4528–4549, 2017.

[45] V. Lakshmanan, K. Hondl, C. K. Potvin, and D. Preignitz, "An improved method for estimating radar echo-top height," *Weather Forecast.*, vol. 28, no. 2, pp. 481–488, 2013.

Husi Letu received the B.S. and M.S. degrees in geography from Inner Mongolia Normal University, Hohhot, China, in 1999 and 2002, and the Ph.D. degree in geosciences and remote sensing from the Center for Environmental Remote Sensing, Chiba University, Chiba, Japan, in 2010.

He was with the Research and Information Center, Tokai University, Tokyo, Japan. He is involved in the algorithm development and validation of the ice cloud product for JAXA's GCOM-C and Himawari-8 satellite missions. He is currently a Professor with the State Key Laboratory of the Science and Remote Sensing, Institute of Remote Sensing and Digital Earth, Chinese Academy of Sciences, Beijing, China. His research interests include atmospheric radiative transfer simulation, light scattering calculation, cloud remote sensing, and ice cloud property retrievals.

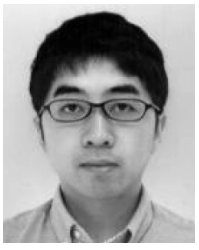

Takashi M. Nagao received the B.E., M.E., and Ph.D. degrees in computer and information science from Nagasaki University, Nagasaki, Japan, in 2004, 2006, and 2010, respectively.

Since 2014, he has been a member with the Earth Observation Research Center, Japan Aerospace Exploration Agency, Tsukuba, Japan.

His research interests include satellite remote sensing of clouds and aerosols, and inverse problem.

Takashi Y. Nakajima received the D.Sc. degree in earth and planetary physics from the University of Tokyo, Tokyo, Japan, in 2002.

He joined Japan Aerospace Exploration Agency, Tsukuba, Japan, in 1994, and moved to Tokai University, Tokyo, in 2005. He was a Visiting Associate Professor with Chiba University, Chiba, Japan, from 2004 to 2007, a Visiting Researcher with the National Institute of Environmental Study, Tsukuba, Japan, from 2005 to 2011, a Visiting Scientist with Colorado State University, Fort Collins, CO, USA, from 2008 to 2009, and a part-time Lecturer with Kyushu University, Fukuoka, Japan, in 2013. He is currently a Professor with Tokai University. His research interests include climate change, remote sensing of clouds and aerosols, and theory of light scattering by nonspherical particle, calculating terrestrial renewable energy.

Dr. Nakajima is a member of JpGU, JMS, RSSJ, AGU, AMS, and OSA. He won the SICE Award in 1998, the Matsumae Shigeyoshi Award, the Horiuchi Award of JMS, the Remote Sensing Society of Japan Award, in 2011.

Jérôme Riedi received the B.S. degree in physics, and the M.S. and Ph.D. degrees in atmospheric sciences from the University of Lille, Villeneuve d'Ascq, France, in 1997, 1998, and 2001, respectively. His Ph.D. research included the use of multiangle and polarization measurements from the POLarization and Directionality of the Earth's Reflectances/Advanced Earth Observation Satellite for determination of cloud microphysical properties.

In 2001, he joined the NASA Goddard Space Flight Center, Greenbelt, MD, USA, where he was a Research Associate at the Goddard Earth Sciences and Technology Center, for one year, focused on MODIS cloud retrievals development and associated product quality assessment. He is currently a Professor with the University of Lille, and also a Research Scientist with the Laboratoire d'Optique Atmosphérique, where he is conducting research on clouds and aerosols properties retrieval with a special emphasis on the use of polarization and the development of a multisensor approach for clouds analysis.

Dr. Riedi is currently a member of the POLDER and GCOM-C/SGLI science teams and the joint ESA/EUMETSAT Science Advisory Group for the Multiviewing-channel-polarisation Imager (3MI) mission in preparation for the European Polar System-Second Generation.

Hiroshi Ishimoto received the Ph.D. degree in science from Kobe University, Kobe, Japan, in 1995.

He has been with the Meteorological Research Institute, Japan Meteorological Agency, Tokyo, Japan, since 1998. His research interests include satellite remote sensing and light scattering by nonspherical atmospheric particles.

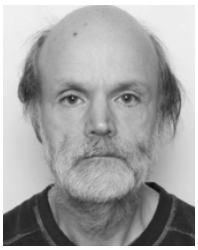

Anthony J. Baran received the Ph.D. degree in atmospheric sciences from London University, London, U.K., with a focus on the radiative and remote sensing properties of cirrus, in 1997.

He was involved in various other fields such as astrophysics, theoretical laser-plasma physics, and stochastic theory applied to wind energy. In 1990, he joined the Met Office, Exeter, U.K., Since then he has remained at the Met Office and is currently also part-employed by the University of Hertfordshire, Hatfield, U.K. He is involved in research covering his research interests. His research interests include scattering and absorption by nonspherical particles, cirrus remote sensing, and radiative transfer. More lately, he has become interested in relating the macrophysics of cirrus to their light scattering properties, very high-resolution measurements of cirrus in the far-IR, and polarimetric measurements of cirrus.

Dr. Baran has also been the Principal Investigator of airborne cirrus campaigns.

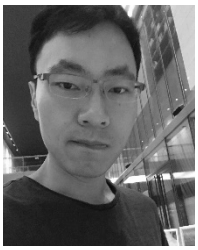

Huazhe Shang received the B.S. degree in remote sensing from Wuhan University, Wuhan, China, in 2011, and the Ph.D. degree in cartography and geographic information system from the University of Chinese Academy of Sciences, Beijing, China, in 2016.

Since 2016, he has been an Assistant Professor of cloud retrieval with the State Key Laboratory of Remote Sensing Science, Institute of Remote Sensing and Digital Earth, Chinese Academy of Sciences, Beijing. His research interests include modeling and remote sensing of clouds.

Miho Sekiguchi received the B.S., M.S., and Ph.D. degrees from the University of Tokyo, Tokyo, Japan, in 1999, 2001, and 2004, respectively.

She is currently an Associate Professor with the Tokyo University of Marine Science and Technology, Tokyo. His research interests include cloud remote sensing, atmospheric radiative transfer, and the earth energy budget.

Maki Kikuchi received the B.S. and M. S. degrees in geophysics from Tohoku University, Sendai, Japan, in 2009 and 2011, respectively. Since 2011, she has been a Researcher and an Engineer with the Earth Observation Research Center, Japan Aerospace Exploration Agency, Tsukuba, Japan. She is involved in the algorithm development and validation of earth, clouds, aerosols and radiation explorer mission. Her research interests include remote sensing of cloud and aerosol and cloud process analysis using satellite observation data.